

Sodium Lignosulfonate-Loaded Halloysite Nanotubes/Epoxy Composites for Corrosion Resistance Coating

Weilin Liu* and Jiansan Li

Cite This: *ACS Omega* 2023, 8, 18425–18434

Read Online

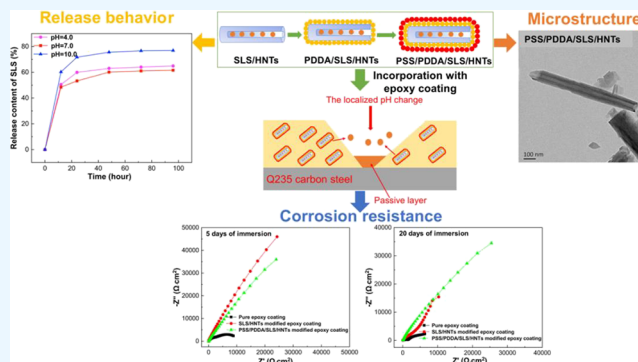
ACCESS |

Metrics & More

Article Recommendations

Supporting Information

ABSTRACT: Corrosion resistance coating applied on Q235 carbon steel in a chloride-rich environment was explored in our research. The coating as a barrier inhibits the penetration of the corrosion medium and provides active corrosion protection for Q235 carbon steel. Halloysite nanotubes (HNTs) were loaded with sodium lignosulfonate (SLS) under vacuum conditions. 4.53% of loading efficiency was validated by thermogravimetric analysis (TGA). The deposition of polyelectrolyte layers including poly(dimethyl diallyl ammonium chloride) (PDDA) and poly(styrenesulfonate) (PSS) not only resulted in controlling the release rate of SLS but also enabled the HNTs to possess pH-responsive release property. The modified HNTs were defined as “PSS/PDDA/SLS/HNTs”, which were characterized by SEM, TEM, FTIR, and zeta potential analyses. TGA elucidates that PSS/PDDA/SLS/HNTs exhibit superior thermal stability. The results of UV–vis spectroscopic analysis confirm that HNTs exhibit a higher release amount in an alkaline medium than in neutral and acidic conditions. Afterward, PSS/PDDA/SLS/HNTs were mixed with the epoxy coating, which was applied on Q235 carbon steel immersed in 3.5 wt % NaCl solution. Electrochemical measurements illustrate the excellent corrosion resistance of the epoxy coating with the addition of PSS/PDDA/SLS/HNTs. Also, water contact angle analysis demonstrates the modification of the epoxy coating with decent hydrophobicity.



1. INTRODUCTION

Q235 carbon steel has been used in a broad range of industries thanks to its excellent mechanical strength and affordable price. However, corrosion, as a critical factor, shortens the service life of carbon steel, especially in a chloride-rich environment, leading to economic losses like repair of corrosion damage and safety problems.¹ In order to mitigate steel corrosion, scholars have proposed some measurements such as corrosion inhibitor,² corrosion-resistant alloyed steel,³ coating,⁴ and cathodic protection.⁵ The methods mentioned above can delay the time of corrosion initiation to a certain extent. However, they may not provide active anticorrosive protection for steel at the corrosion sites, which will impose a constraint on application.

During the corrosion process, the corrosion site of the metal will form a corrosion cell consisting of a micro-anode and a micro-cathode, which is accompanied by a localized pH change of the corrosive medium. Hydrolysis of metal ions at the anode area decreases the localized pH, while the oxygen reduction reaction at the cathode area causes an increase in the localized pH. Therefore, it is urgent to develop an effective strategy that can inhibit steel corrosion once the environment changes. One approach is that adding a “smart” carrier loaded with a corrosion inhibitor into coating guarantees the required corrosion protection when and where needed.^{6,7} These carriers

are sensitive to specific stimuli such as pH, temperature, mechanical damage, and light.^{8,9} Once the carriers are triggered by the variation of the above parameters, they will release corrosion inhibitors intelligently. In addition, the storage of inhibitors in carriers can not only inhibit the detrimental interaction between the component of the inhibitor and coating constituents but also can solve the issue of early inhibitor leaching, thereby prolonging the life span of coating.^{10,11}

Several nanocarriers, such as halloysite nanotubes,¹² carbon nanotubes,¹³ mesoporous silica,¹⁴ and calcium carbonate,¹⁵ have been applied to encapsulate materials like corrosion inhibitors and drugs because of their hollow inner lumens. Nanocomposite materials become research hotspots due to their great loading capacity and self-assembled property. Different self-assembled methods endow nanocomposite materials with various styles. Guo et al. synthesized sandwiched

Received: December 6, 2022

Accepted: April 28, 2023

Published: May 15, 2023



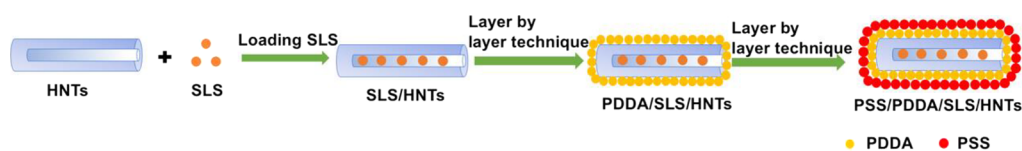


Figure 1. Schematic illustration of preparation of PSS/PDDA/SLS/HNTs.

nanocomposites using Fe_3O_4 nanoparticles, poly(allylamine) hydrochloride molecules, and carboxylate graphene oxide sheets via layer-by-layer techniques.¹⁶ Xing et al. combined electrospinning and thermal treatment to obtain poly-(vinylalcohol)/poly(acrylic acid)/carboxylate graphene oxide nanosheet@polydopamine used in wastewater treatment.¹⁷

Jiao et al. prepared reduced graphene oxide/chitosan/silver nanoparticle composites with porous 3D nanostructures via the self-assembly process and in situ reduction approach.¹⁸

Compared to the above carriers, halloysite nanotubes (HNTs) have promising applications in storing the active molecules due to their ecofriendliness, cost-effectiveness, good loading capacity, and biocompatibility.^{12,19} HNTs with many superior advantages have been used as nanocontainers to load antimicrobial agents, corrosion inhibitors, proteins, and drugs.^{20–22} Furthermore, the inner and outer surfaces of HNTs show a difference in surface charge, allowing them to modify the surface easily.²³ As for the HNT structure, the positively charged internal alumina layer facilitates the loading of negative inhibitors in the hollow lumen of HNTs. Also, the positively charged polyelectrolyte could be absorbed on the negative external surface of the HNTs.²⁴

For the purpose of controlling the release of inhibitors, several functionalized methods were applied to encapsulate the pore outlet of HNTs with the aid of supramolecular layers: (i) forming an end stopper at the end of HNTs^{25,26} and (ii) absorbing polymers on the HNT surface.^{27,28} When HNTs are triggered by stimuli like pH, they will intelligently open or block the pore mouth of HNTs. For example, the controlled release of corrosion inhibitors from HNTs under a specific pH value can be realized by the deposition of polyelectrolyte layers on the HNT surface. Shchukin et al. applied HNTs to load 2-mercaptobenzothiazole as the corrosion inhibitor and the release of inhibitor triggered by pH, which was controlled by polyelectrolyte multilayers of poly(allylamine hydrochloride) and poly(styrene sulfonate) on the HNT surface.²⁹ Khan et al. developed hybrid halloysite nanotubes (HHNTs) impregnated with a corrosion inhibitor (imidazole), and another inhibitor (dodecylamine) was intercalated into the polyelectrolyte layers containing polyethylenimine and sulfonated, which shows efficient release when pH changes in the corrosive medium.

Sodium lignosulfonate, as a byproduct of acid sulfite pulp mills, has a wide range of applications like dispersing agents in concrete admixture industry and additives in oil well drilling.³⁰ As an anionic surfactant, it contains active groups like sulfonic, phenylic hydroxyl, and carbon chains, leading to a certain degree of surface activity.³¹ Hence, it can absorb on the metal surface and show a promising application of corrosion protection of metals. SLS was reported to be an ecofriendly inhibitor for the corrosion inhibition of zinc, carbon steel, and magnesium alloy.^{32–34} The coordination of lone pairs on carbonyl oxygen and metal ions will generate a stable complex and thus enhance the corrosion inhibition of metals against corrosive agents.³⁵ Furthermore, SLS with a negative charge is

conductive to load in the lumen of HNTs with a positive charge.

Limited research has been carried out on the application of HNTs as carriers for environmentally friendly corrosion inhibitors. Inspired by the aforementioned research, we proposed pH-responsive HNTs involving SLS as a corrosion inhibitor for the loading of PDDA and PSS as polyelectrolyte layers for controlling the release of SLS from the lumen of HNTs intelligently. The morphology, structure, and thermal property of modified HNTs were evaluated by SEM, TEM, FTIR, and TGA, while the release behavior of SLS in solutions with various pH was analyzed by UV–vis spectroscopic analysis. Moreover, the corrosion protection effect of epoxy coatings added with modified HNTs was investigated by electrochemical measurements and the water contact angle test.

2. EXPERIMENTAL SECTION

2.1. Materials and Sample Preparation. Q235 carbon steel plates (0.002 wt % S, 0.003 wt % N, 0.021 wt % P, 0.021 wt % O, 0.13 wt % C, 0.17 wt % Si, 0.57 wt % Mn, and balance Fe) with the dimension of 120 mm × 50 mm × 0.5 mm were used for electrochemical measurements. The steel samples were ground with a metallographic paper and sonicated in ethanol for 3 min to remove organic contaminants, followed by rinsing with distilled water.

2.2. Synthesis of PSS/PDDA/SLS/HNTs. Figure 1 displays a schematic diagram of preparation steps including inhibitor loading and absorption of polyelectrolyte layers. 2 g of SLS (purchased from Macklin, China) was first dissolved in 30 mL of distilled water; then, 1 g of HNTs (provided by Xian Mingchuan Co., Ltd., China) was dispersed into the above solution under stirring. After that, the suspension was placed in a vacuum jar under vacuum condition for 2 h, and then the system was restored to atmospheric pressure. The above procedure was repeated four times to increase the SLS loading. Subsequently, the suspension was taken out and centrifugation was carried out with a speed of 9000 rpm for 7 min to obtain SLS/HNTs from the solution. The prepared SLS/HNTs were rinsed with distilled water and dried at 50 °C for 24 h.

The process of the preparation of PSS/PDDA/SLS/HNTs is as follows: 1 mL of 35 wt % PDDA solution (obtained from Macklin, China) was added to 99 mL of distilled water and stirred for 10 min. 4 g of PSS powder (obtained from Aladdin, China) was dispersed in distilled water (96 mL) under continuous stirring with the help of a magnetic stirrer. 1.5 g of SLS/HNT powder was mixed with the prepared 30 mL of PDDA solution, stirring for 15 min, followed by the addition of 0.5 g of NaCl (purchased from Aladdin, China). Centrifugation was used to separate the excess water and PDDA from SLS/HNTs. The second layer of PSS was absorbed on the SLS/HNT surface as in the above procedure to synthesize PSS/PDDA/SLS/HNTs.

2.3. Preparation of Epoxy Coating. Epoxy resin and hardener were obtained from Zhejiang Danbao Resin Co., Ltd.,

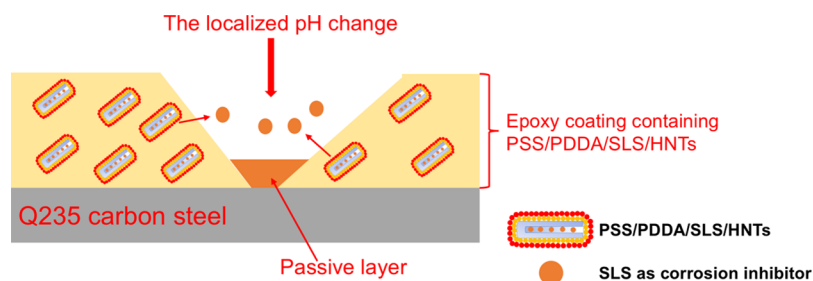


Figure 2. Schematic representation of epoxy coating containing PSS/PDDA/SLS/HNTs.

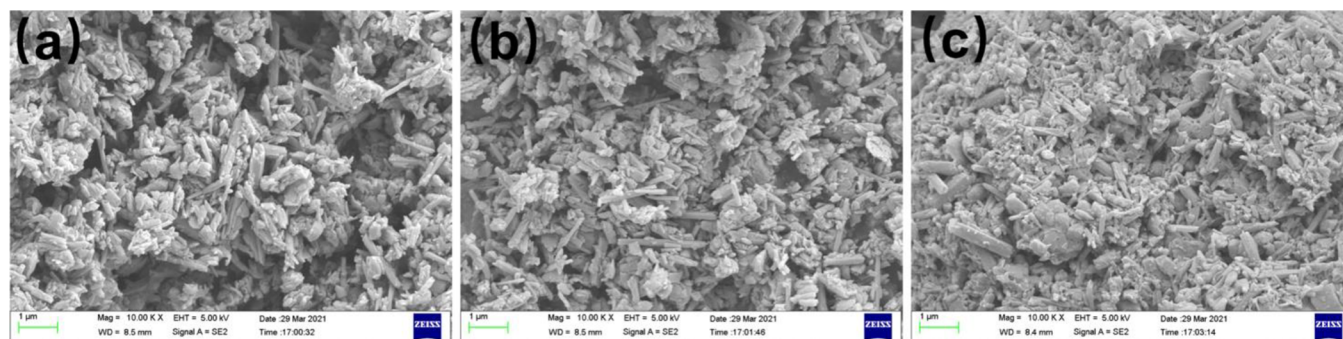


Figure 3. SEM micrographs of (a) HNTs, (b) SLS/HNTs, and (c) PSS/PDDA/SLS/HNTs.

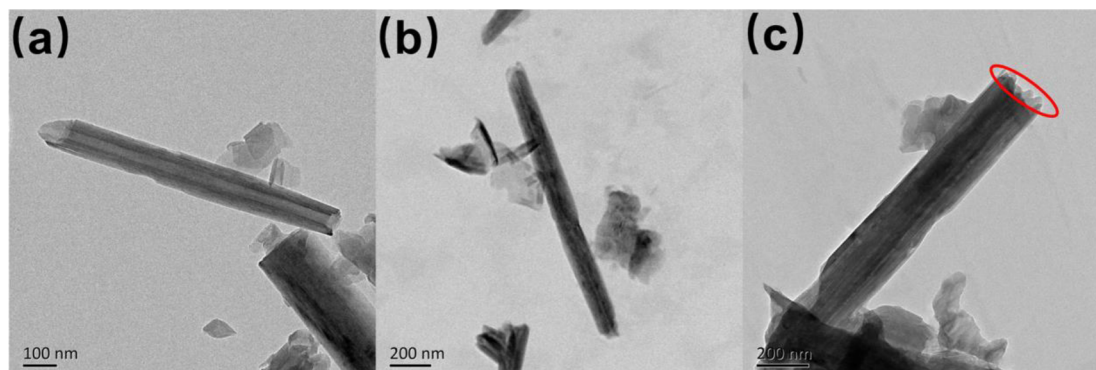


Figure 4. TEM images of (a) HNTs, (b) SLS/HNTs, and (c) PSS/PDDA/SLS/HNTs.

China. To fabricate the modified epoxy coatings, fillers including SLS/HNTs and PSS/PDDA/SLS/HNTs were added into epoxy resin, respectively. First, 1 g of filler was dispersed into 3 g of ethanol, which was ultrasonically agitated for 20 min. The mixed solution was dispersed in 5 g of epoxy resin and mechanically stirred for 10 min at a speed of 500 rpm. Then, 5 g of hardener was mixed with the above mixture and stirred for 10 min at 500 rpm. The epoxy mixture was transferred into the vacuum chamber to remove the bubble. Q235 carbon steel plates were painted with a pure epoxy coating and modified epoxy coatings, respectively, and cured for 7 days at ambient temperature to obtain a dry film. The thickness of coatings was controlled at around 130 μm . The corrosion resistance mechanism of the epoxy coating containing PSS/PDDA/SLS/HNTs is schematically displayed in Figure 2. The release of SLS can be triggered by a localized pH change. A passive layer forms on Q235 carbon steel after the absorption of SLS. The cross-sectioned modified epoxy coating samples were obtained after placing them in liquid nitrogen, as presented in Figure S1. It is obviously noticed that SLS/HNTs and PSS/PDDA/SLS/HNTs are uniformly

distributed in the epoxy coating. Hence, these fillers show excellent dispersibility in the epoxy mixture.

2.4. Characterization. The loading of SLS in the HNTs and the thermal stability of SLS/HNTs were verified through TGA (NETZSCH, TG209F1, Germany) in the temperature range of 30–650 °C at a heating rate of 20 °C/min, using nitrogen atmosphere. Also, whether the polyelectrolyte layers absorb on the HNT surface was confirmed by FTIR analysis (Bruker, VERTEX 70, USA). The morphology of HNTs, SLS/HNTs, and PSS/PDDA/SLS/HNTs was characterized by SEM (ZEISS, Merlin, Germany) and TEM (JEOL, JEM 2100F, Japan). Cross-sectional morphologies of the modified epoxy coatings were also observed using SEM. A UV–vis spectrophotometer (Yoke, UV755B, China) was applied to study the release of SLS from PSS/PDDA/SLS/HNTs under various pH values (pH = 4.0, 7.0, and 10.0). The potential of each layer of the HNTs was analyzed by a zeta potential equipment (HORIBA, SZ-100Z, Japan). The corrosion protection performance of the modified epoxy coating in 3.5 wt % NaCl solution was characterized by means of electrochemical measurements including electrochemical impedance

spectroscopy (EIS) and potentiodynamic polarization testing, using an electrochemical workstation (Princeton, 263A, USA) at room temperature in the 10 mHz–100 kHz frequency range with a sinusoidal perturbation of 10 mV. A three-electrode system was introduced in which the Q235 carbon steel with an exposed area of 1 cm² served as a working electrode, a saturated calomel electrode was used as a counter electrode, and a platinum electrode was employed as a reference electrode. The obtained EIS result was fitted employing ZSimpWin software. Tafel polarization curves were obtained in the potential range of ± 250 mV with respect to the open-circuit potential at the scan rate of 1 mV/s. Hydrophobicity analysis of coatings was performed using a contact angle tester (Dataphysics, OCA40 Micro, Germany).

3. RESULTS AND DISCUSSION

3.1. SEM Analysis. The SEM micrographs of the HNTs and modified HNTs are illustrated in Figure 3. HNTs with a tubular structure were mixed with some flaky impurities (Figure 3a). The entrapment of SLS into the HNTs exhibited no obvious morphology difference compared with the HNTs without loading (Figure 3b), while the SEM image of PSS/PDDA/SLS/HNTs displayed a similar morphology as that of HNTs and SLS/HNTs (Figure 3c).

3.2. TEM Analysis. The morphology of HNTs, SLS/HNTs, and PSS/PDDA/SLS/HNTs was observed by TEM, as shown in Figure 4. HNTs display a tubular structure with a length range of 800–1400 nm, while the inner diameter of the hollow lumen is about 50 nm. A comparison of the morphological images of HNTs and SLS/HNTs (Figure 4a,b) demonstrates that the structure of HNTs remained unchanged even after loading with SLS. Comparing the inner space of HNTs and SLS/HNTs, the latter one was observed to become dark, showing that SLS had been successfully loaded into HNTs. Smooth polyelectrolyte layers, as marked by circles, can be found on the surface of PSS/PDDA/SLS/HNTs (Figure 4c).

3.3. FTIR Spectra. Figure 5 shows the FTIR spectra of HNTs, SLS, SLS/HNTs, and PSS/PDDA/SLS/HNTs. Massive hydroxyl groups exist on the inner and outer surfaces of HNTs, which are linked with Al atoms and Si atoms, respectively. A schematic of the HNT structure is displayed in Figure S2. HNT-related peaks seen are as follows. The absorption bands at 3696 and 3623 cm⁻¹ depict the stretching

vibration of the Al–OH bond on the inner surface of HNTs.³⁶ The O–H stretching of water in the HNTs is detected by the absorption peaks at 1646 cm⁻¹.³⁷ Si–O–Si stretching at the outer surface of HNTs is seen at the wavenumber of 1034 cm⁻¹.³⁸ The observed peak at 910 cm⁻¹ corresponds to the bending vibration of Al–OH.³⁹ The characteristic peak at 538 cm⁻¹ originated from Al–O–Si deformation.⁴⁰ As for the FTIR spectra of SLS, there is a characteristic peak at 1513 cm⁻¹ ascribed to the vibration of the aromatic benzene ring.⁴¹ Additionally, an S=O stretching vibration is found at 1046 cm⁻¹. The peak at 1513 cm⁻¹ can also be seen in the FTIR spectrum of SLS/HNTs, which confirms the entrapment of SLS into the HNT structure. The characterized peak of S=O could not be distinguished in the SLS/HNT spectrum, which overlaps with the broad and robust peak of pristine HNTs. In the case of PSS/PDDA/SLS/HNTs, the new characteristic peak at 2927 and 2855 cm⁻¹ represents C–H elastic vibration, which can be ascribed to PSS. The enhanced peak is located at 1640 cm⁻¹ due to the stretching vibration of cyano group in PDDA. Compared with HNTs, the appearance of new characteristic peaks in the FTIR spectra verifies the successful absorption of polyelectrolyte layers on PSS/PDDA/SLS/HNTs.

3.4. Thermal Stability of SLS/HNTs. Figure 6 displays the TGA and differential thermogravimetric analysis (DTA) curves of SLS and three kinds of HNTs. There are two stages of weight loss in the TGA curves of HNTs and SLS/HNTs. According to Figure 6a, the initial weight loss stage was below 400 °C, which is attributed to the absorbed water molecules in the multiwalls of HNTs.⁴² The second mass loss in the temperature range of 400–650 °C could be corresponded to the dehydroxylation of HNTs at a high temperature.⁴³ No obvious weight loss was noticed in HNTs within 30–650 °C. The total weight loss of HNTs was about 15.14%, confirming that they have great thermal stability due to a slight weight loss. As for SLS, it exhibits three weight loss stages from 30 to 650 °C. Exothermic reaction at the 30–200 °C range is attributed to water loss. The sulfonic acid group and hydroxyl group demonstrate significant exothermic weight loss in the range of 200–450 °C. The mass loss seen in the range of 450–650 °C is assigned to the pyrolysis of aromatic rings. Two steps of weight loss were seen in the TGA curve of SLS/HNTs. Meanwhile, the exothermic peaks of SLS/HNTs are centered at 60 and 500 °C, as similar as that of HNTs (Figure 6b). An exothermic peak at 60 °C is connected to water molecules' evaporation. In the 300–400 °C range, SLS/HNTs demonstrate weight loss unlike HNTs without loading, which is related to the thermal decomposition of SLS.⁴⁴ The second weight loss linked with the thermal decomposition of HNTs with an exothermic peak is located at 500 °C. There is no remarkable weight loss in SLS/HNTs from 30 to 650 °C. In terms of PSS/PDDA/SLS/HNTs, the weight loss below 250 °C is considered to be due to the loss of absorbed water. A moderate change in weight loss of PSS/PDDA/SLS/HNTs can be seen in the range of 250–430 °C in comparison with that of HNTs and SLS/HNTs, which is attributed to the decomposition of PSS and PDDA. Weight loss occurred between 430 and 650 °C due to the dehydroxylation of HNTs. In comparison with the DTG curve of SLS/HNTs, the shift of the endothermic peak from 500 to 475 °C can be witnessed on PSS/PDDA/SLS/HNTs, which is connected to the decomposition of the polyelectrolyte layer. 22.03% weight loss happened in the temperature region of 30–650 °C. The

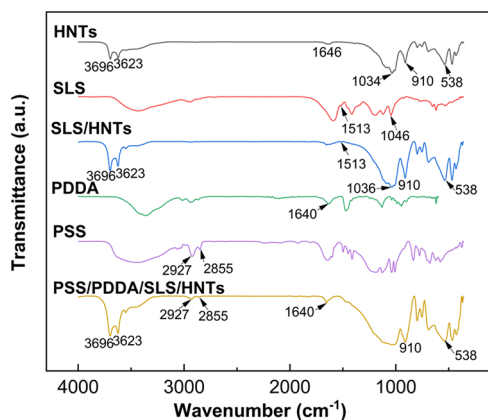


Figure 5. FTIR spectra of HNTs, SLS, SLS/HNTs, PDDA, PSS, and PSS/PDDA/SLS/HNTs.

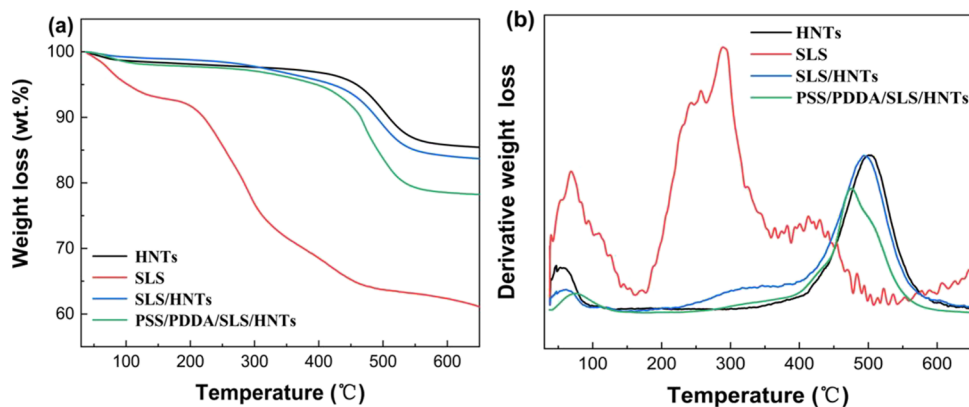


Figure 6. (a) TGA and (b) DTG plots of HNTs, SLS, SLS/HNTs, and PSS/PDDA/SLS/HNTs.

thermal analysis of PSS/PDDA/SLS/HNTs confirms that they have a wide application in the industry field due to their superior thermal stability. The loading efficiency of SLS/HNTs was 4.53%, which can be calculated by eq 1:

$$W_{\text{SLS/HNTs}} = \eta W_{\text{SLS}} + (1 - \eta) W_{\text{HNTs}} \quad (1)$$

where $W_{\text{SLS/HNTs}}$, W_{SLS} , and W_{HNTs} represent the weight loss of SLS/HNTs, SLS, and HNTs, respectively. η denotes the loading capacity of SLS/HNTs. 17.32, 63.25, and 15.14% weight loss of SLS/HNTs, SLS, and HNTs can be obtained from the TGA and DTG curves.

3.5. Zeta Potential Analysis. The zeta potential values of SLS/HNTs, PDDA/SLS/HNTs, and PSS/PDDA/SLS/HNTs are depicted in Figure 7. The outer and inner surfaces of

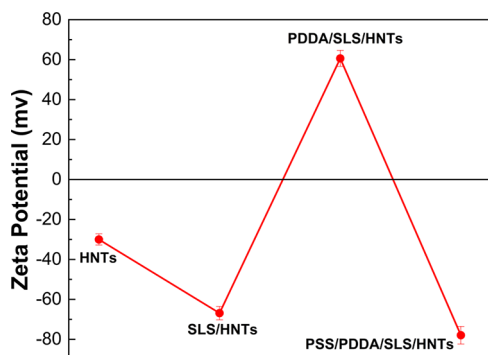


Figure 7. Zeta potential charge on HNTs, SLS/HNTs, PDDA/SLS/HNTs, and PSS/PDDA/SLS/HNTs.

HNTs with opposite zeta potential values allow them to possess multifunctionality.⁴⁵ A large number of siloxane groups (Si–O–Si) exist on the HNT surface with an aluminosilicate multiwall tubular structure, whereas the inner lumen of HNTs is composed of Al–OH groups.⁴⁶ HNTs have an inner lumen with positive charges and an outer surface with negative charges as a result of their unique structural features. Due to the fact that the inner lumen of HNTs encapsulated negatively charged SLS, the zeta potential of SLS/HNTs (−68.12 mV) was much more negative than that of pristine HNTs (−30 mV).⁴⁷ Therefore, positively charged materials can be used to modify the negative SLS/HNT surface. After the attachment of the positively charged PDDA to the SLS/HNT surface, the zeta potential significantly shifted toward a positive value (60.63 mV). Furthermore, after the precipitation of PSS, the zeta potential moves toward a negative direction, reaching

−77.94 mV. Polyelectrolyte layers have already successfully deposited on the SLS/HNT surface, which can be clearly observed from the zeta potential variation after each polyelectrolyte layer's absorption.

3.6. Release Kinetics of SLS from PSS/PDDA/SLS/HNTs. A UV–vis spectrophotometer was used to measure the absorbance of the solution in the wavelength range of 800–190 nm. In order to calculate the release amount of the inhibitor, the concentration–absorbance equation of SLS was investigated by monitoring the absorbance at 280 nm where SLS shows an absorption peak. The obtained concentration–absorbance equation of SLS is as follows:

$$y = 0.0038x - 0.0405 \quad (2)$$

where x denotes the concentration of SLS and y is the absorbance intensity.

HNTs loaded with SLS were added into the solution with various pH values (4.0, 7.0, and 10.0). The above solution was prepared using solutions with 0.1 mol/L NaCl. Acetic acid or sodium hydroxide was applied to adjust the pH value of the solution. The release profiles of SLS/HNTs at pH 4.0, 7.0, and 10.0 as a function of time (12, 24, 48, 72, and 96 h) are depicted in Figure 8. In the first 12 h, SLS/HNTs at different pH values exhibit a higher release rate. With the elongation of immersion time, the release rate of SLS from SLS/HNTs demonstrates a downward trend. Notably, the release amount of SLS at pH 10.0 was higher than that at pH 4.0 and 7.0 throughout the testing period. After 48 h, the release of SLS at different pH values reaches equilibrium and exhibits no

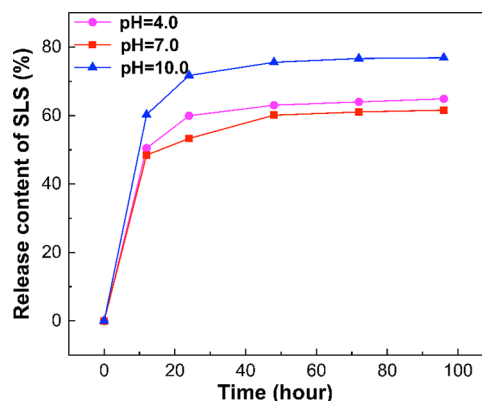


Figure 8. Release profile of PSS/PDDA/SLS/HNTs at various pH values.

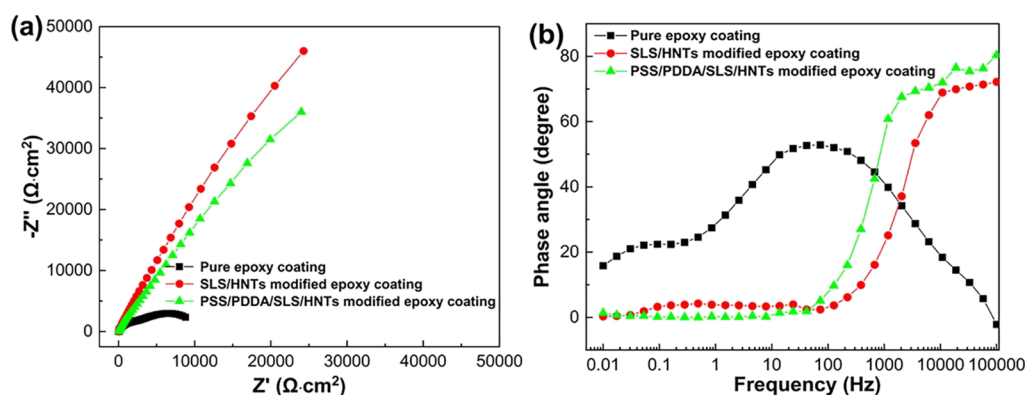


Figure 9. EIS plots: (a) Nyquist and (b) bode-phase angle for Q235 carbon steel of pure and modified epoxy coating after 5 days of exposure in 3.5 wt % NaCl solution.

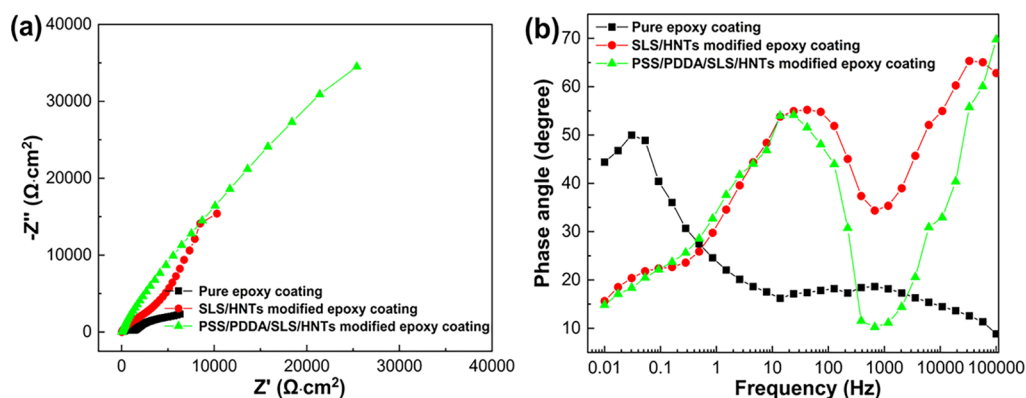


Figure 10. EIS plots: (a) Nyquist and (b) bode-phase angle for Q235 carbon steel of pure and modified epoxy coating after 20 days of exposure in 3.5 wt % NaCl solution.

Table 1. EIS Fitting Data for Pure and Modified Epoxy Coating on Q235 Carbon Steel Immersed in 3.5 wt % NaCl Solution

epoxy coating	time (day)	R_s ($\Omega\cdot\text{cm}^2$)	CPE_{coat} ($\Omega^{-1}\cdot\text{cm}^{-2}\cdot\text{s}^n$)	n_1	R_{coat} ($\Omega\cdot\text{cm}^2$)	CPE_{dl} ($\Omega^{-1}\cdot\text{cm}^{-2}\cdot\text{s}^n$)	n_2	R_{ct} ($\Omega\cdot\text{cm}^2$)
pure		51.71	$7.50\text{E}-5$	0.85	3563	$5.02\text{E}-4$	0.77	7146
SLS/HNTs	5	31.68	$1.46\text{E}-4$	0.79	$2.18\text{E}+5$			
PSS/PDDA/SLS/HNTs		28.65	$1.50\text{E}-4$	0.77	$1.09\text{E}+5$			
pure		44.85	$1.92\text{E}-5$	0.45	1511	$3.39\text{E}-4$	0.65	6034
SLS/HNTs	20	22.13	$9.21\text{E}-5$	0.76	6381	$4.29\text{E}-4$	0.77	$4.47\text{E}+4$
PSS/PDDA/SLS/HNTs		35.23	$9.09\text{E}-5$	0.83	$1.19\text{E}+4$	$4.85\text{E}-5$	0.79	$1.91\text{E}+5$

increase. 75.58% of SLS release amount was witnessed at pH 10.0, while the cumulative release at pH 4.0 and 7.0 was 63.02 and 60.13%, respectively. Compared with neutral and acidic conditions, a higher release content of SLS is noticed in alkaline medium, which may be attributed to the following reasons. SLS penetrates the microholes on the polyelectrolyte layer into solution, so the compactness of the polyelectrolyte layer has a significant influence on the release behavior of SLS.²⁴ Based on the electrostatic attraction between cationic (PDDA) and anionic polyelectrolytes (PSS), double polyelectrolyte layers on the HNT surface were synthesized via a layer-by-layer technique.⁴⁸ The ionization degree of the polyelectrolyte changes with the variation of pH, leading to the polyelectrolyte layer with different structures and charge density. In an alkaline medium, PSS with stronger structural rigidity is unfavorable for creating a dense polyelectrolyte layer.⁴⁹ Moreover, the shrink of molecular chain of PDDA was witnessed in an alkaline medium as a result of increased charge density. A polyelectrolyte layer containing PDDA has loose

structures and microholes due to the desorption of PDDA on the HNT surface. Hence, SLS exhibits efficient release in an alkaline environment.

3.7. Corrosion Resistance of As-Received Sodium Lignosulfonate-Loaded Halloysite Nanotubes/Epoxy Composites. The EIS plots of epoxy coating containing SLS/HNTs or PSS/PDDA/SLS/HNTs in 3.5 wt % NaCl solution for 5 days and 20 days are depicted in Figures 9 and 10, respectively. The larger capacitive loop diameter of the coated steel sample in the Nyquist plots represents the better anticorrosion performance it has.⁵⁰ Both modified epoxy coatings have significantly larger capacitive loop diameters than the pure epoxy coating during 20 days of immersion (Figures 9a and 10a). A decline in capacitive loop diameter was experienced in all coatings when the immersion time reached 20 days.

Generally speaking, the number of response peaks represents the number of time constants. In the initial stage of immersion, Bode-phase angle plots (Figure 9b) for modified epoxy

coatings comprise a single response peak, which was fitted by the equivalent circuit with one time constant (Figure S3a), while two response peaks presented in the pure epoxy coating were fitted using an equivalent circuit with two time constants (Figure S3b). When the immersion time reached 20 days, two response peaks appeared in all epoxy coatings (Figure 10b), and therefore an equivalent circuit with two time constants was applied to fit them. Fitted electrochemical parameters related to three kinds of epoxy coatings are listed in Table 1. The fitted EIS parameters consist of the solution resistance (R_s), the resistance of coating (R_{coat}), the capacitance of coating (CPE_{coat}), charge-transfer resistance (R_{ct}), and double-layer capacitance of steel (CPE_{dl}).⁵¹ Due to surface heterogeneity, the steel surface possesses non-ideal capacitance properties. Ideal capacitance was replaced by the constant phase element.⁵²

Time constant present at different frequency regions reflects the barrier property of coating. High-frequency time constant (10^4 – 10^5 Hz) is evidence of the protective effect of the coating, whereas the time constant at the intermediate frequency range (1 – 10^3 Hz) demonstrates the corrosion initiation of steel due to microcracks in the coating. A low-frequency time constant (10^{-2} – 1 Hz) is assigned to the corrosion activity at the coating/steel interface.⁵³ One time constant at the high-frequency range is observed in modified epoxy coatings after 5 days of immersion, illustrating that modified epoxy coatings, as a barrier, prevent the corrosive medium like chloride ions from being absorbed on the steel surface at the beginning of immersion. Although the time constant appearing at the intermediate frequency range for all coating samples suggests the micropores in coatings after 20 days of exposure to 3.5 wt % NaCl solution, both modified epoxy coatings still show high-frequency time constants, demonstrating that they are capable of hindering chloride ions from reaching the steel surface. The reason for the presence of micropores in coatings is that increasing water molecules penetrated into the coatings at longer immersion times. As for the pure epoxy coating, the second time constant presenting at the low-frequency range is attributed to the formation of corrosion products on the steel surface.

Generally speaking, the R_{coat} value gradually decreases with the extension of immersion time due to the corrosive electrolytes penetrating through the coatings. All epoxy coatings show a decline in R_{coat} value, which is caused by a significant accumulation of chloride ions at the interface between the metal and coating. Under the immersion time of 5 days, the value of R_{coat} for SLS/HNT-modified epoxy coating is higher than that of PSS/PDDA/SLS/HNT-modified epoxy coating because polyelectrolyte layers prolong the release of the inhibitor. As the immersion time increases to 20 days, PSS/PDDA/SLS/HNT-modified epoxy coating has a higher R_{coat} value than the SLS/HNT-modified epoxy coating, which is attributed to the continuous release of SLS from PSS/PDDA/SLS/HNTs and the early leaching of SLS/HNTs. Water absorption of coating can be characterized by CPE_{coat} . With the further extending immersion time (20 days), three kinds of epoxy coatings witnessed a decline in the CPE_{coat} value as a result of the nonhomogeneous diffusion of corrosive media into the coating/steel interface. Continuous permeation of sodium chloride solution will cause blister and defects on the coating. Once a certain amount of chloride ions accumulate on the coating/steel interface, corrosion occurs in steel. With the gradual ingress of corrosive species, the corrosion behavior of

the coating/steel system is under the control of R_{ct} value. A higher R_{ct} value of coating demonstrates a lower probability of corrosion.⁵³ After 20 days of exposure to chloride environment, the R_{ct} value of epoxy coating added with PSS/PDDA/SLS/HNTs ($1.91\text{E}+5 \Omega\cdot\text{cm}^2$) was found to be approximately 2 orders of magnitude higher than that of pure epoxy coating ($6034 \Omega\cdot\text{cm}^2$), evidencing the excellent corrosion resistance in the presence of PSS/PDDA/SLS/HNTs. The CPE_{dl} value demonstrates the stabilization and delamination of the coating/steel interface.⁵⁴ The lowest CPE_{dl} value ($4.85\text{E}-5 \Omega^{-1}\cdot\text{cm}^2\cdot\text{s}^n$) can be witnessed in the epoxy coating containing PSS/PDDA/SLS/HNTs, confirming the decent compatibility of the coating and steel surface. These results also elucidate that the addition of PSS/PDDA/SLS/HNTs can promote the stabilization of the coating/steel interface. To summarize, excellent corrosion resistance performance is witnessed in the epoxy coating containing PSS/PDDA/SLS/HNTs.

The Tafel polarization plots of pure and modified epoxy coatings are depicted in Figure 11. The related electrochemical

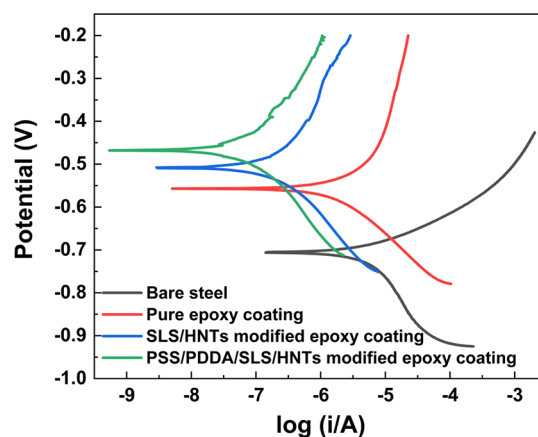


Figure 11. Tafel curves for bare steel and different epoxy coatings after immersion in 3.5 wt % NaCl solution for 20 days.

parameters acquired from the polarization curves are summarized in Table 2. Lower corrosion current density (i_{corr}) and higher corrosion potential (E_{corr}) represent a better barrier effect of coating. Obviously, the i_{corr} value of pure epoxy coating ($5.611\text{E}-7 \text{ A}\cdot\text{cm}^2$) is lower (over 1 order of magnitude) than that of PSS/PDDA/SLS/HNT-modified epoxy coating ($1.786\text{E}-8 \text{ A}\cdot\text{cm}^2$). As for the corrosion potential, the maximum one is witnessed on the epoxy coating with PSS/PDDA/SLS/HNTs, reaching -0.466 V. Polarization resistance (R_p), corrosion rate (v_{corr}), and corrosion protection efficiency (CPE) are calculated by eqs 3–5, respectively

$$R_p = \frac{\beta_a \cdot \beta_c}{2.303(\beta_a + \beta_c) i_{\text{corr}}} \quad (3)$$

$$v_{\text{corr}} = \frac{A i_{\text{corr}}}{n\rho F} \times 87,600 \quad (4)$$

$$\text{CPE} (\%) = \frac{i_{\text{corr}}^0 - i_{\text{corr}}^c}{i_{\text{corr}}^0} \times 100\% \quad (5)$$

where β_a and β_c represent the anode and cathode Tafel slopes, A denotes the formula weight of iron, n is the chemical valence of Fe^{2+} , ρ represents the iron density (g/cm^3), F denotes the

Table 2. Tafel Electrochemical Parameters for Coating Samples on Q235 Carbon Steel Exposed to 3.5 wt % NaCl Solution for 20 days

coating samples	E_{corr} (V)	i_{corr} (A·cm ²)	β_a	β_c	R_p (k Ω ·cm ²)	$\nu_{\text{corr}} \times 10^{-3}$ (mm·a ⁻¹)	CPE (%)
bare steel	-0.708	3.761E-6	0.897	5.705	0.896	43.69	
pure	-0.555	5.611E-7	11.77	15.62	5.195	6.830	89.95
SLS/HNTs	-0.508	5.636E-8	188.17	131.64	596.310	0.687	98.50
PSS/PDDA/SLS/HNTs	-0.466	1.786E-8	418.47	357.58	4677.385	0.218	99.52

Faraday constant, and i_{corr}^0 and i_{corr}^c are the corrosion current densities of bare steel and coated steel, respectively.

R_p reflects the physical barrier property of epoxy coatings. PSS/PDDA/SLS/HNT-modified epoxy coating shows the largest R_p value of 4677.385 k Ω ·cm², which is significantly higher than that of SLS/HNT-modified epoxy coating (596.310 k Ω ·cm²) and pure epoxy coating (5.195 k Ω ·cm²). In terms of corrosion rate, epoxy coating containing PSS/PDDA/SLS/HNTs (0.218×10^{-3} mm·a⁻¹) shows a lower rate than SLS/HNT-modified epoxy coating (0.687×10^{-3} mm·a⁻¹) after 20 days of immersion. The corrosion rate is 1 order of magnitude higher for pure epoxy coating (6.830×10^{-3} mm·a⁻¹) compared to modified epoxy coating. The incorporation of PSS/PDDA/SLS/HNTs into epoxy coating leads to an appreciable increase in corrosion protection efficiency, reaching 99.52%. It was found that the CPE values of pure epoxy coating and SLS/HNTs are 89.95% and 98.50%, respectively. The above result demonstrated that the addition of PSS/PDDA/SLS/HNTs could enhance the corrosion resistance of epoxy coating in a chloride-rich environment.

The water contact angle of pure and modified epoxy coating is shown in Figure S4. The lowest water contact angle of 80.9° is witnessed in pure epoxy coating (Figure S4a). A contact angle of 96.7° can be seen in the SLS/HNT-modified epoxy coating (Figure S4b). Meanwhile, after the addition of PSS/PDDA/SLS/HNTs in the epoxy coating, the contact angle grew to 102.4° (Figure S4c). The enhanced hydrophobicity was observed in PSS/PDDA/SLS/HNT-modified epoxy coating. The addition of chloride ions into a polyelectrolyte solution enables PDDA and PSS to possess stronger structural rigidity and present common-ion effect, leading to the weakened ionization effect of the polyelectrolyte. Since the molecular coils become tighter, some charge was embedded, and the number of charges that existed on the polyelectrolyte layer decreased. PSS/PDDA/SLS/HNTs could play a crucial role in improving the hydrophobicity and preventing corrosive agents from penetrating into the coating.

4. CONCLUSIONS

In this work, SLS was encapsulated into the inner lumen of HNTs under a vacuum condition. The adsorption of polyelectrolyte layers including PDDA and PSS on the HNT surface was achieved through a layer-by-layer technique. The successful loading of SLS was confirmed by the appearance of new characteristic peaks in the FTIR spectra and the morphological change in TEM images. The loading efficiency of SLS/HNTs was 4.53%, and PSS/PDDA/SLS/HNTs showed great thermal stability, which can be acquired from TGA. After the deposition of each layer, the shift of zeta potential proves that polyelectrolyte layers have been successfully deposited on the surface of HNTs. UV-vis spectroscopic analysis of the time-dependent release of SLS from HNTs shows a higher release amount of SLS in an alkaline medium. Later, the modified HNTs were introduced

in the epoxy coating applied on Q235 carbon steel. Superior corrosion resistance of epoxy coating containing PSS/PDDA/SLS/HNTs in 3.5 wt % NaCl solution was elucidated by the results of electrochemical measurements and water contact angles.

■ ASSOCIATED CONTENT

Supporting Information

The Supporting Information is available free of charge at <https://pubs.acs.org/doi/10.1021/acsomega.2c07786>.

Cross-sectional SEM micrograph of epoxy coating containing SLS/HNTs or PSS/PDDA/SLS/HNTs; schematic representation of the crystalline structure of HNTs; equivalent circuits used for fitting EIS data of three kinds of epoxy coatings immersed in 3.5 wt % NaCl solution; and water contact angles of pure and modified epoxy coatings (PDF)

■ AUTHOR INFORMATION

Corresponding Author

Weilin Liu – School of Engineering and Information Technology, University of New South Wales, Canberra, ACT 2600, Australia; orcid.org/0000-0001-5576-9034; Email: lweilin2021@163.com

Author

Jiansan Li – College of Mechanical and Automotive Engineering, South China University of Technology, Guangzhou 510640, China

Complete contact information is available at: <https://pubs.acs.org/10.1021/acsomega.2c07786>

Notes

The authors declare no competing financial interest.

■ ACKNOWLEDGMENTS

This work was supported by the Special Fund Project of Guangdong Province (Grant No. B2190150).

■ REFERENCES

- (1) Subbiah, K.; Lee, H. S.; Mandal, S.; Park, T. Conifer Cone (*Pinus Resinosa*) as a Green Corrosion Inhibitor for Steel Rebar in Chloride-Contaminated Synthetic Concrete Pore Solutions. *ACS Appl. Mater. Interfaces* **2021**, *13*, 43676–43695.
- (2) Wu, M.; Ma, H. F.; Shi, J. J. Enhanced Corrosion Resistance of Reinforcing Steels in Simulated Concrete Pore Solution With Low Molybdate to Chloride Ratios. *Cem. Concr. Compos.* **2020**, *110*, No. 103589.
- (3) Zhang, L.; Niu, D. T.; Wen, B.; Fu, Q.; Peng, G.; Su, L.; Blackwood, D. J. Initial-Corrosion Condition Behavior of the Cr and Al Alloy Steel Bars in Coral Concrete for Marine Construction. *Cem. Concr. Compos.* **2021**, *120*, No. 104051.
- (4) Chen, Y.; Xia, C.; Shepard, Z.; Smith, N.; Rice, N.; Peterson, A. M.; Sakulich, A. Self-Healing Coatings for Steel-Reinforced Concrete. *ACS Sustainable Chem. Eng.* **2017**, *5*, 3955–3962.

- (5) Polder, R. B.; Peelen, W. H. A.; Stoop, B. T. J.; Neeft, E. A. C. Early Stage Beneficial Effects of Cathodic Protection in Concrete Structures. *Mater. Corros.* **2011**, *62*, 105–110.
- (6) Khan, A.; Hassanein, A.; Habib, S.; Nawaz, M.; Shakoore, R. A.; Kahraman, R. Hybrid Halloysite Nanotubes a Smart Carriers for Corrosion Protection. *ACS Appl. Mater. Interfaces* **2020**, *12*, 37571–37584.
- (7) Snihrova, D.; Lamaka, S. V.; Montemor, M. F. “SMART” Protective Ability of Water Based Epoxy Coatings Loaded with CaCO₃ Microbeads Impregnated With Corrosion Inhibitors Applied on AA2024 Substrates. *Electrochim. Acta* **2012**, *83*, 439–447.
- (8) Yamuna, J.; Siva, T.; Kumari, S. S. S.; Sathiyarayanan, S. A Smart Poly(aniline-formaldehyde) Microcapsule Based Self-Healing Anticorrosive Coating. *RSC Adv.* **2016**, *6*, 79–86.
- (9) Shchukina, E.; Shchukin, D.; Grigoriev, D. Effect of Inhibitor-Loaded Halloysites and Mesoporous Silica Nanocontainers on Corrosion Protection of Powder Coatings. *Prog. Org. Coat.* **2017**, *102*, 60–65.
- (10) Fu, X.; Du, W. B.; Dou, H. X.; Fan, Y.; Xu, J. N.; Tian, L. M.; Zhao, J.; Ren, L. Q. Nanofiber Composite Coating with Self-Healing and Active Anticorrosive Performances. *ACS Appl. Mater. Interfaces* **2021**, *13*, 57880–57892.
- (11) Akhondi, M.; Jamalzadeh, E. Fabrication of Beta-Cyclodextrin Modified Halloysite Nanocapsules for Controlled Release of Corrosion Inhibitors in Self-Healing Epoxy Coatings. *Prog. Org. Coat.* **2020**, *145*, No. 105676.
- (12) Joshi, A.; Abdullayev, E.; Vasiliev, A.; Volkova, O.; Lvov, Y. Interfacial Modification of Clay Nanotubes for the Sustained Release of Corrosion Inhibitors. *Langmuir* **2013**, *29*, 7439–7448.
- (13) Wang, W.; Li, W. H.; Fan, W. J.; Zhang, X. Y.; Song, L. Y.; Xiong, C. S.; Gao, X.; Liu, X. J. Accelerated Self-Healing Performance of Magnetic Gradient Coating. *Chem. Eng. J.* **2018**, *332*, 658–670.
- (14) Borisova, D.; Mohwald, H.; Shchukin, D. G. Mesoporous Silica Nanoparticles for Active Corrosion Protection. *ACS Nano* **2011**, *5*, 1939–1946.
- (15) Raj, R.; Morozov, Y.; Calado, L. M.; Taryba, M. G.; Kahraman, R.; Shakoore, R. A.; Montemor, M. F. Calcium Carbonate Particles Loaded with Triethanolamine and Polyethylenimine for Enhanced Corrosion Protection of Epoxy Coated Steel. *Corros. Sci.* **2020**, *167*, No. 108548.
- (16) Guo, R.; Jiao, T. F.; Li, R. F.; Chen, Y.; Guo, W. H.; Zhang, L. X.; Zhou, J. X.; Zhang, Q. R.; Peng, Q. M. Sandwiched Fe₃O₄/Carboxylate Graphene Oxide Nanostructures Constructed by Layer-by-Layer Assembly for Highly Efficient and Magnetically Recyclable Dye Removal. *ACS Sustainable Chem. Eng.* **2017**, *6*, 1279–1288.
- (17) Xing, R. T.; Wang, W.; Jiao, T. F.; Ma, K.; Zhang, Q. R.; Hong, W.; Qiu, H.; Zhou, J. X.; Zhang, L. X.; Peng, Q. M. Bioinspired Polydopamine Sheathed Nanofibers Containing Carboxylate Graphene Oxide Nanosheet for High-Efficient Dyes Scavenger. *ACS Sustainable Chem. Eng.* **2017**, *5*, 4948–4956.
- (18) Jiao, T. F.; Zhao, H.; Zhou, J. X.; Zhang, Q. R.; Luo, X. N.; Hu, J.; Peng, Q. M.; Yan, X. H. Self-Assembly Reduced Graphene Oxide Nanosheet Hydrogel Fabrication by Anchorage of Chitosan/Silver and Its Potential Efficient Application toward Dye Degradation for Wastewater Treatments. *ACS Sustainable Chem. Eng.* **2015**, *3*, 3130–3139.
- (19) Lvov, Y.; Panchal, A.; Fu, Y.; Fakhrullin, R.; Kryuchkova, M.; Batasheva, S.; Stavitskaya, A.; Glotov, A.; Vinokurov, V. Interfacial Self-Assembly in Halloysite Nanotube Composites. *Langmuir* **2019**, *35*, 8646–8657.
- (20) Cavallaro, G.; Lazzara, G.; Massaro, M.; Milioto, S.; Noto, R.; Parisi, F.; Riela, S. Biocompatible Poly(N-isopropylacrylamide)-Halloysite Nanotubes for Thermoresponsive Curcumin Release. *J. Phys. Chem. C* **2015**, *119*, 8944–8951.
- (21) Xing, X. T.; Xu, X. Y.; Wang, J. H.; Hu, W. B. Preparation, Release and Anticorrosion Behavior of a Multi-Corrosion Inhibitors-Halloysite Nanocomposite. *Chem. Phys. Lett.* **2019**, *718*, 69–73.
- (22) Lvov, Y.; Abdullayev, E. Functional Polymer-Clay Nanotube Composites with Sustained Release of Chemical Agents. *Prog. Polym. Sci.* **2013**, *38*, 1690–1719.
- (23) Kumar, S. S.; Kakooei, S.; Ismail, M. C.; Haris, M. Synthesis and Characterization of Metal Ion End Capped Nanocontainer Loaded with Duo Green Corrosion Inhibitors. *J. Mater. Res. Technol.* **2020**, *9*, 8350–8354.
- (24) Lvov, Y. M.; Shchukin, D. G.; Möhwald, H.; Price, R. R. Halloysite Clay Nanotubes for Controlled Release of Protective Agents. *ACS Nano* **2008**, *2*, 814–820.
- (25) Xing, X. T.; Zhou, D.; Tang, E. J.; Liu, S. J.; Chu, X. M.; Xu, X. D.; Xu, Y. Q. A Novel Method to Control the Release Rate of Halloysite Encapsulated Na₂MoO₄ with Ca²⁺ and Corrosion Resistance for Q235 Steel. *Appl. Clay Sci.* **2020**, *188*, No. 105492.
- (26) Wang, M.; Wang, J. H.; Hu, W. Preparation and Corrosion Behavior of Cu-8-HQ@HNTs/Epoxy Coating. *Prog. Org. Coat.* **2020**, *139*, No. 105434.
- (27) Yang, Y. T.; Chen, Y.; Leng, F.; Huang, L.; Wang, Z. J.; Tian, W. Q. Recent Advances on Surface Modification of Halloysite Nanotubes for Multifunctional Applications. *Appl. Sci.* **2017**, *7*, 1215.
- (28) Xu, D.; Lou, C.; Huang, J.; Lu, X.; Xin, Z.; Zhou, C. L. Effect of Inhibitor-Loaded Halloysite Nanotubes on Active Corrosion Protection of Polybenzoxazine Coatings on Mild Steel. *Prog. Org. Coat.* **2019**, *134*, 126–133.
- (29) Shchukin, D. G.; Lamaka, S. V.; Yasakau, K. A.; Zheludkevich, M. L.; Ferreira, M. G. S.; Mohwald, H. Active Anticorrosion Coatings with Halloysite Nanocontainers. *J. Phys. Chem. C* **2008**, *112*, 958–964.
- (30) Ouyang, X. Q.; Lou, H. M.; Yang, D. J. Corrosion and Scale Inhibition Properties of Sodium Lignosulfonate and Its Potential Application in Recirculating Cooling Water System. *Ind. Eng. Chem. Res.* **2006**, *45*, 5716–5721.
- (31) Qiu, X. Q.; Kong, Q.; Zhou, M. S.; Yang, D. J. Aggregation Behavior of Sodium Lignosulfonate in Water Solution. *J. Phys. Chem. B* **2010**, *114*, 15857–15861.
- (32) Xiao, T.; Dang, N.; Hou, L. F.; Wei, Y. H.; Guo, C. L.; Du, H. Y. Inhibiting Effect of Sodium Lignosulfonate on the Corrosion of AZ31 Magnesium Alloy in NaCl Solution. *Rare Met. Mater. Eng.* **2016**, *45*, 1600–1604.
- (33) Li, J. S.; Liu, W. L.; Xie, W. C. Influence of Sodium Lignosulfonate on the Corrosion-Inhibition Behavior of Q235 Steel in Simulated Concrete Pore Solutions. *Int. J. Electrochem. Sci.* **2020**, *15*, 7136–7151.
- (34) Li, X. H.; Deng, S. D.; Du, G. B.; Xie, X. G. Synergistic Inhibition Effect of Walnut Green Husk Extract and Sodium Lignosulfonate on the Corrosion of Cold Rolled Steel in Phosphoric Acid Solution. *J. Taiwan Inst. Chem. Eng.* **2020**, *114*, 263–283.
- (35) Ahangar, M.; Izadi, M.; Shahrabi, T.; Mohammadi, I. The Synergistic Effect of Zinc Acetate on the Protective Behavior of Sodium Lignosulfonate for Corrosion Prevention of Mild Steel in 3.5 wt% NaCl Electrolyte: Surface and Electrochemical Studies. *J. Mol. Liq.* **2020**, *314*, No. 113617.
- (36) Zhang, J. Y.; Zhang, Y. T.; Chen, Y. F.; Du, L.; Zhang, B.; Zhang, H. Q.; Liu, J. D.; Wang, K. J. Preparation and Characterization of Novel Polyethersulfone Hybrid Ultrafiltration Membranes Bending with Modified Halloysite Nanotubes Loaded with Silver Nanoparticles. *Ind. Eng. Chem. Res.* **2012**, *51*, 3081–3090.
- (37) Ren, T. T.; Tang, G. W.; Yuan, B.; Yang, Y.; Yan, Z. S.; Ma, L. R.; Huang, X. Hexadecyltrimethoxysilane-Modified SiO₂ Nanoparticle-Coated Halloysite Nanotubes Embedded in Silicone-Acrylic Polymer Films as Durable Fluorine-Free Superhydrophobic Coatings. *ACS Appl. Nano Mater.* **2020**, *3*, 5807–5815.
- (38) Yu, D.; Wang, J.; Hu, W.; Guo, R. Preparation and Controlled Release Behavior of Halloysite/2-mercaptobenzothiazole Nanocomposite with Calcined Halloysite as Nanocontainer. *Mater. Des.* **2017**, *129*, 103–110.
- (39) Xing, X. T.; Wang, J. H.; Li, Q. S.; Hu, W. B.; Yuan, J. A Novel Acid-Responsive HNTs-Based Corrosion Inhibitor for Protection of Carbon Steel. *Colloids Surf., A* **2018**, *553*, 295–304.

(40) Xing, W. N.; Ni, L.; Huo, P. W.; Lu, Z. Y.; Liu, X. L.; Luo, Y. Y.; Yan, Y. S. Preparation High Photocatalytic Activity of CdS/Halloysite Nanotubes (HNTs) Nanocomposites with Hydrothermal Method. *Appl. Surf. Sci.* **2012**, *259*, 698–704.

(41) Liu, W. L.; Li, J. S.; Huang, X. Q.; Bi, J. Y. Corrosion Protection of Q235 Steel Using Epoxy Coatings Loaded with Calcium Carbonate Microparticles Modified by Sodium Lignosulfonate in Simulated Concrete Pore Solutions. *Materials* **2021**, *14*, 1982.

(42) Askari, F.; Ghasemi, E.; Ramezanzadeh, B.; Mahdavian, M. Synthesis and Characterization of the Fourth Generation of Zinc Phosphate Pigment in the Presence of Benzotriazole. *Dyes Pigm.* **2016**, *124*, 18–26.

(43) Izadi, M.; Mohammadi, I.; Shahrabi, T.; Ramezanzadeh, B.; Fateh, A. Corrosion Inhibition Performance of Novel Eco-Friendly Nanoreservoirs as Bi-Component Active System on Mild Steel in Aqueous Chloride Solution. *J. Taiwan Inst. Chem. Eng.* **2019**, *95*, 555–568.

(44) Banu, D.; El-Aghoury, A.; Feldman, D. Contributions to Characterization of Poly(vinyl chloride)-Lignin Blends. *J. Appl. Polym. Sci.* **2006**, *101*, 2732–2748.

(45) Lvov, Y.; Price, R.; Gaber, B.; Ichinose, I. Thin Film Nanofabrication via Layer-by-Layer Adsorption of Tubule Halloysite, Spherical Silica, Proteins and Polycations. *Colloids Surf., A* **2002**, *198*, 375–382.

(46) Jia, Y. L.; Qiu, T.; Guo, L. H.; Ye, J.; He, L. F.; Li, X. Y. Reduction-Coagulation Preparation of Hybrid Nanoparticles of Graphene and Halloysite Nanotubes for Use in Anticorrosive Waterborne Polymer Coatings. *ACS Appl. Nano Mater.* **2018**, *1*, 1541–1550.

(47) Lvov, Y.; Wang, W.; Zhang, L.; Fakhruddin, R. Halloysite Clay Nanotubes for Loading and Sustained Release of Functional Compounds. *Adv. Mater.* **2016**, *28*, 1227–1250.

(48) Li, L. L.; Takada, A.; Ma, W.; Fujikawa, S.; Ariyoshi, M.; Igata, K.; Okajima, M.; Kaneko, T.; Takahara, A. Structure and Properties of Hybrid Film Fabricated by Spin-Assisted Layer-by-Layer Assembly of Sacran and Imogolite Nanotubes. *Langmuir* **2020**, *36*, 1718–1726.

(49) Schonhoff, M. Self-Assembled Polyelectrolyte Multilayers. *Curr. Opin. Colloid Interface Sci.* **2003**, *8*, 86–95.

(50) Shen, L.; Li, Y.; Zhao, W. J.; Miao, L. J.; Xie, W. P.; Lu, H. M.; Wang, K. Corrosion Protection of Graphene-Modified Zinc-Rich Epoxy Coatings in Dilute NaCl Solution. *ACS Appl. Nano Mater.* **2019**, *2*, 180–190.

(51) Liu, H. W.; Xu, D. K.; Yang, K.; Liu, H. F.; Cheng, Y. F. Corrosion of Antibacterial Cu-Bearing 316L Stainless Steels in the Presence of Sulfate Reducing Bacteria. *Corros. Sci.* **2018**, *132*, 46–55.

(52) Majd, M. T.; Shahrabi, T.; Ramezanzadeh, B. Low Carbon Steel Surface Modification by an Effective Corrosion Protective Nanocomposite Film Based on Neodymium-Polyacrylic Acid-Benzimidazole. *J. Alloys Compd.* **2019**, *783*, 952–968.

(53) Raj, R.; Morozov, Y.; Calado, L. M.; Taryba, M. G.; Kahraman, R.; Shakoor, A.; Montemor, M. F. Inhibitor Loaded Calcium Carbonate Microparticles for Corrosion Protection of Epoxy-Coated Carbon Steel. *Electrochim. Acta* **2019**, *319*, 801–812.

(54) Hao, Y. S.; Sani, L. A.; Ge, T. J.; Fang, Q. H. Phytic Acid Doped Polyaniline Containing Epoxy Coatings for Corrosion Protection of Q235 Carbon Steel. *Appl. Surf. Sci.* **2017**, *419*, 826–837.